ARTICLE

Metallopolymer Capacitor in "One Pot" by Self-Directed UV-Assisted Process

Vijaykumar S. Ijeri,[†] Jijeesh R. Nair,[†] Claudio Gerbaldi,*[,‡] Roberta M. Bongiovanni,[†] and Nerino Penazzi[†]

Department of Materials Science and Chemical Engineering, Politecnico di Torino, C.so Duca degli Abruzzi 24, 10129 Turin, Italy, and IIT@POLITO Center for Space Human Robotics, Italian Institute of Technology, C.so Trento 21, 10129 Turin, Italy

ABSTRACT Silver metalized methacrylate films are prepared by single-step UV curing process with good conductivity on both sides. The major component of the composite is Bisphenol A ethoxylate dimethacrylate, which can be photopolymerized by a photoreactive initiator under UV light. Under the same conditions of UV irradiation, silver ions are deposited as metal nanoparticles while the pyrrole is oxidized to polypyrrole. The migration of silver ions and pyrrole toward both surfaces during polymerization leads to the formation of a metallo-polymer capacitor. The composite films are characterized by SEM-EDX and electrical measurements for possible applications as capacitors in flexible and/or nonplanar electronics.

KEYWORDS: capacitors • conducting polymers • flexible electronics • organic–inorganic hybrid composites • photopolymerization • silver nanoparticles

INTRODUCTION

The technological need for new and better soft materials, as well as the drive for new knowledge and fundamental understanding has led to significant advances in the field of polymer nanocomposites. They combine typical properties of organic polymers (e.g., elasticity, dielectrical properties, etc.) with the advantages of nanoparticles, particularly, the high specific surface area. The specific properties of nanoparticles can be used in technical preparation methods that are compatible to micro technology, if they can be embedded in thin films. Silver is the optimum metal in optics and microelectronics because it has an unmatched reflection coefficient and the highest electrical conductivity of all metals (1, 2).

The current widespread interest in silver–metalized polymeric materials is driven largely by their potential applications in printed circuit boards, contact devices in microelectronics, flexible polymer electronics (3–5), catalysis (6–8), space applications (9), etc. Silver-polymer nanocomposites have been studied with the purpose of enhancing the dielectric constant for applications in embedded capacitors as well (10–12).

Some well-known deposition methods, such as physical vapor deposition (PVD, sputtering or vacuum evaporation), chemical vapor deposition (CVD), electrodeposition, and electroless chemical reduction, involve the external deposition of the metallic phase onto the substrate surface. Metallization of polymeric films by these established techniques often involves two to three stages. First, the substrate film is prepared; second, the surface of the base film is modified via plasma, ion beam, electron beam, photolytic, or chemical treatments to enhance metal-substrate adhesion; finally, the metal is deposited onto the film surface. Apart from being laborious, a major problem of such procedures is adhesion. The adhesion to polymers of passive metals (e.g., silver, gold, copper, etc.) is notoriously poor (1, 13). To overcome this problem, Southward and others developed in situ, single-stage self-metallization procedures, wherein the film formation involves an internal thermally induced reduction of silver(I) from a single homogeneous solution that contains both the organometallic silver complex and the desired polyimide precursor (1, 3, 14–16).

Most of the studies related to surface silvering are focused on polyimides and restricted to a single surface. There is only one report of double surface silvering of polyimides by Qi et al.: they used the process of ion exchange on damp-dried films of polyamic acid to get silver polyamates on the surface (13). The films were then thermally cured over a period of about 4 h with temperatures ranging from 135 to 300 °C. Thermal curing induced cycloimidization of the polyamic acid precursor to the polyimide form and reduction of silver(I) to silver metal, giving metalized surfaces.

Free-radical photopolymerization (UV-curing) is a well established polymerization technique that takes place under UV light to obtain a highly cross-linked polymeric thermoset matrix. The process is well-known for being fast and environmentally friendly. We have previously demonstrated the use of this versatile technique to prepare plasticized polymer membranes for Li-ion batteries application in a single step (17–19).

* Corresponding author. Tel.: (+39) 011 090 3402. Fax: (+39) 011 090 3401. E-mail: claudio.gerbaldi@iit.it or claudio.gerbaldi@polito.it.
Received for review July 28, 2010 and accepted September 17, 2010
[†] Politecnico di Torino.
[‡] Italian Institute of Technology.
DOI: 10.1021/am1006639

Published on Web 10/15/2010

Table 1. Compositions of Reactive Mixtures[a]

sample	pyrrole (g)	$AgNO_3$ (g)	pyrrole:$AgNO_3$ (mole ratio)	$CH_3OH + H_2O$ (g)
1	0.25	0.318	2:1	1.25
2	0.25	0.318	2:1	0.63
3	0.25	0.159	4:1	0.63
4	0.25	0.079	8:1	0.63
5	0.12	0.079	4:1	0.63
6	0.12	0.079	4:1	0.63[b]
7	0.06	0.079	2:1	0.63

[a] The amounts of BEMA and initiator were 1.86 and 0.075 g, respectively, in all formulations. [b] In this formulation, NMP was used instead of methanol + water mixture.

Here we report the first example of dual surface nanosilvering of a methacrylate polymer film by a simple one-pot UV-curing process. By the term "one-pot" we mean a procedure in which the metalized film is directly developed from a single homogeneous solution that contains both the native metal precursor (i.e., Ag^+) and the desired reactive precursors of the final polymeric network. That is, the sample is obtained in a single stage and no subsequent distinct metallization stage is involved. To the best of our knowledge, such an approach has not been reported so far. This kind of polymeric film metalized on both sides is conceptually a capacitor, well-suited for flexible and/or nonplanar electronics. The samples have been characterized by SEM-EDX and electrical measurements.

EXPERIMENTAL SECTION

Unless otherwise stated, all starting materials and reagents were purchased from commercial suppliers and used without any further purification. Experiments were repeated two to three times and were found to be reproducible. All samples were stored in ambient laboratory conditions.

Materials. The reactive formulation for the preparation of conducting polymer composite films was based on a dimethacrylic monomer: Bisphenol A ethoxylate (15 EO/phenol) dimethacrylate (BEMA, average $M_n = 1700$, Aldrich). The photoinitiator was 2-hydroxy-2-methyl-1-phenyl-1-propanone (Darocur 1173, Ciba Specialty Chemicals). Silver nitrate ($AgNO_3$, 99.5%), methanol (CH_3OH, 99.8%), and pyrrole (C_4H_5N, ≥ 98%) from Aldrich were used as such.

Photopolymerization Procedure. The reactive formulations were prepared as shown in the Table 1.

$AgNO_3$ was dissolved in 50% (v/v) $CH_3OH + H_2O$ mixture (this methanol + water mixture enabled the dissolution of silver nitrate and pyrrole and homogenized the mixture with BEMA and initiator). To this solution, BEMA, pyrrole and initiator were added subsequently and mixed thoroughly. A molar ratio of 2:1 or higher for pyrrole to silver nitrate was maintained to ensure complete reduction of Ag(I) and also to study the effects of changing compositions (20). The mixtures were then poured into Petri dishes and exposed to UV-radiation for 3 min on each side. The photochemical curing was performed by using a medium vapor pressure Hg UV lamp (Helios Italquartz, Italy),

Scheme 1. Schematic Representation of the One-Pot UV-Curing Procedure

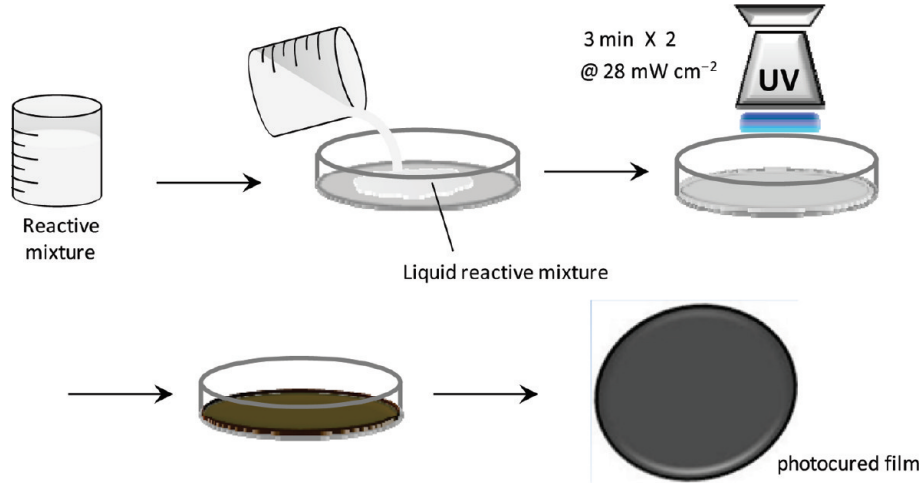

Scheme 2. Schematic Illustration of the One-Pot UV-Curing Process to Self-Directed Dual Surface Polymer Metallization

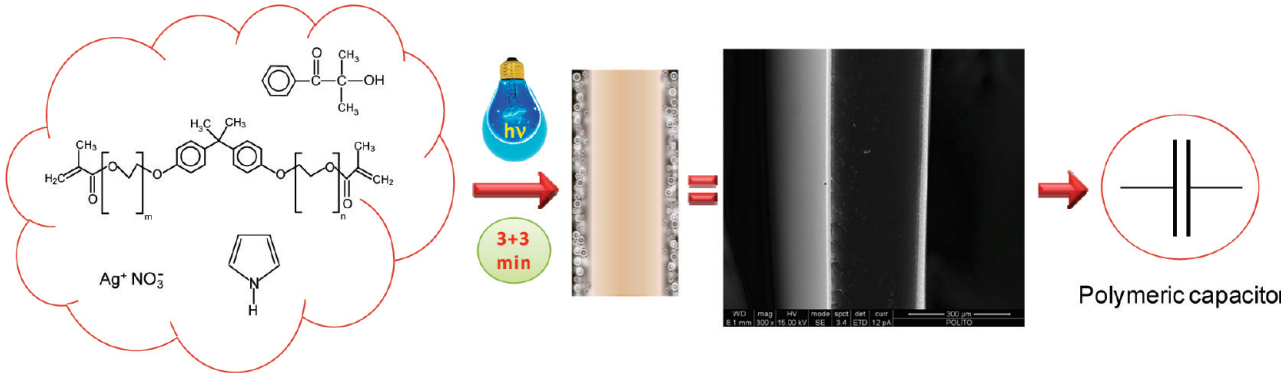

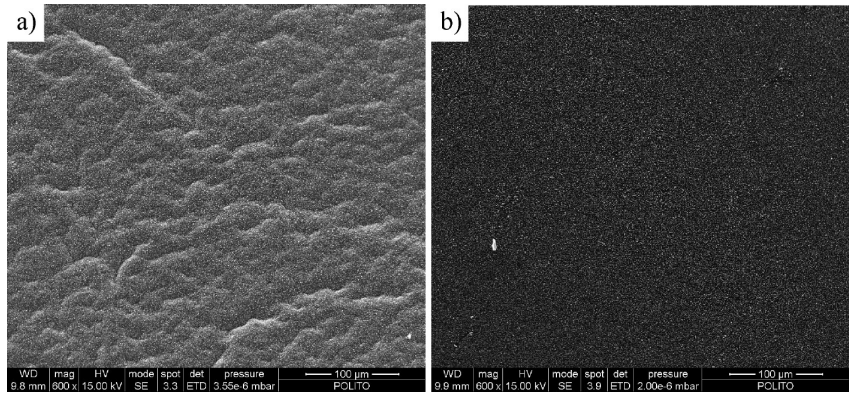

FIGURE 1. SEM micrographs of sample 1: (a) top surface (exposed first), (b) bottom surface (exposed next). Ag nanoparticles embedded in polypyrrole are clearly visible on both surfaces.

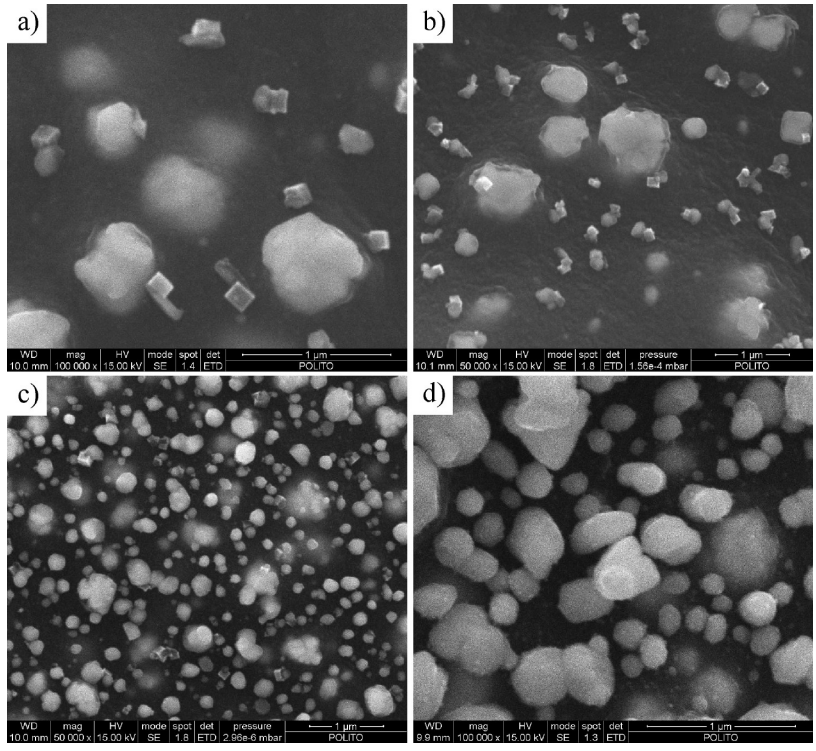

FIGURE 2. SEM micrographs of the top surfaces (exposed first) of (a) sample 2, (b) sample 3, (c) sample 5, and (d) sample 7.

with a radiation intensity on the surface of the sample of 28 ± 2 mW cm^{-2}. For this process, the samples were held under a pure N_2 atmosphere in small sealed boxes equipped with a quartz window. These conditions ensure maximum curing (disappearance of the methacrylic double bonds, checked by FT-IR) (17). Free films were easily detached from the dishes. They are referred in the text as sample 1, 2, 3, etc. The process sequence for the single-pot synthesis of silvered membranes is shown schematically in Scheme 1.

In the absence of UV light (i.e., under ambient laboratory conditions), the reaction between silver nitrate and pyrrole is very slow, and the black color of polypyrrole formation starts to be visible after about an hour (20). Also, there is no film formation, as BEMA does not polymerize in absence of UV.

SEM Analysis. Morphological characterization of the films was performed employing a FEI Quanta Inspect 200LV scanning electron microscope (SEM, max magnification of 1.5×10^5) equipped with an energy-dispersive X-ray analyzer EDAX Genesis system with SUTW detector. Prior to analysis, all the samples were coated with about 8 nm of Cr to minimize the effect of the electron beam irradiation which may possibly lead to charging and "burning" of the polymer network. The samples for the cross-sectional scanning electron microscopy (SEM) images were prepared by fracturing the given film in liquid nitrogen in order to avoid any change in the morphology.

Electrical Measurements. The surface resistances of the films were calculated from the current−voltage (I−V) curves recorded by a CHI 760 D Electrochemical Workstation, with constant pressure spring loaded gold-plated pin probes (spring force 1.26 N, contact resistance 50 mΩ, P25−0822 Flat Head, Harwin). There was a fixed distance of 1.0 cm between the probes, and measurements were made at 5 different points on the surface of the films.

The same electrochemical workstation was used to obtain the capacitance−voltage plots. Circular discs of 1 cm in diameter were cut out from the samples (thickness = 500 ± 25 μm) and sandwiched between two flat stainless steel (SS-316) cylindrical electrodes (resistance of less than 1 ohm) in Teflon-made Swagelok test cells. Capacitance was measured as a function of applied potential in the range of ±1.0 V at a fixed frequency of 100 Hz. As the surface resistance of sample 6 was too high,

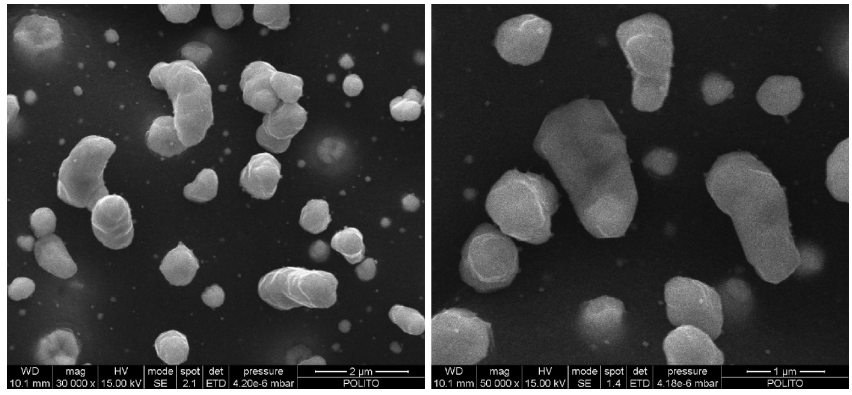

FIGURE 3. SEM micrographs of the top surface (exposed first) of sample 6 at different magnifications.

Table 2. Summary of Top Surface SEM-EDX Analysis[a]

sample	remarks[b]	C:Ag (wt % ratio)	C:Ag (at % ratio)
1	Ag nanocubes and agglomerates	50.87:49.13	90.29:09.71
2	same as above	53.88:46.12	91.30:08.70
3	same as above (but more clumped together)	57.08:42.92	92.27:07.73
4	Ag nanoparticles and agglomerates (dense)	33.95:64.05	83.44:16.56
5	Ag nanoparticles and agglomerates (dense)	43.00:57.00	87.14:12.86
6	rod- or bean-shaped clusters (spread out)	66.15:33.85	94.61:05.39
7	Ag nanoparticles and agglomerates (most dense)	25.45:74.55	75.41:24.59

[a] An area of 5 μm × 5 μm was used for EDX analysis. [b] Readers may refer to Figures 2 and 3 for the corresponding SEM images.

it was coated with few dots of conducting silver paint for these measurements.

RESULTS AND DISCUSSION

Preparation. The major component of the composite is Bisphenol A ethoxylate dimethacrylate (BEMA), which can be photopolymerized by a photoreactive initiator under UV light. The complete process involves multiple reactions, simultaneously. A schematic representation is shown in Scheme 2.

On irradiation with UV, the initiator generates radicals by intramolecular scission; then, the monomer BEMA undergoes free radical polymerization, the details of which have been already discussed (17−19). Under the same conditions of UV irradiation, silver ions are reduced to metallic form while the pyrrole is oxidized to polypyrrole. All these reactions occur within a few minutes. This process gave methacrylate films with one side conducting surface of 7−10 μm composed mostly of silver nanoparticles and polypyrrole. Interestingly, when the sample is turned over to expose the other surface to UV light, we get a polymer film with both sides silvered to more or less the same extent. This interesting and intriguing phenomenon forms the core of the present communication.

Seven kinds of samples were prepared with the compositions as shown in Table 1 to understand the effects of different components. Detailed procedures for synthesis and characterization are provided in the Experimental Section.

SEM-EDX Characterization. Scanning electron micrographs of the top and bottom surfaces of sample 1 are shown in Figure 1.

The top surface, which was exposed to UV first, shows the characteristic wrinkles of polypyrrole. The top surfaces of the other samples prepared were all similar but the wrinkles were less prominent as the amount of pyrrole added decreased in subsequent samples. The bottom surfaces do not show such wrinkles, because they were in contact with glass for the first 3 min, while the top surface was exposed to UV. They were then turned over and exposed for the next 3 min. For all the samples, both the top and bottom surfaces have the Ag nanoparticles more or less evenly distributed and embedded in the polymer matrix.

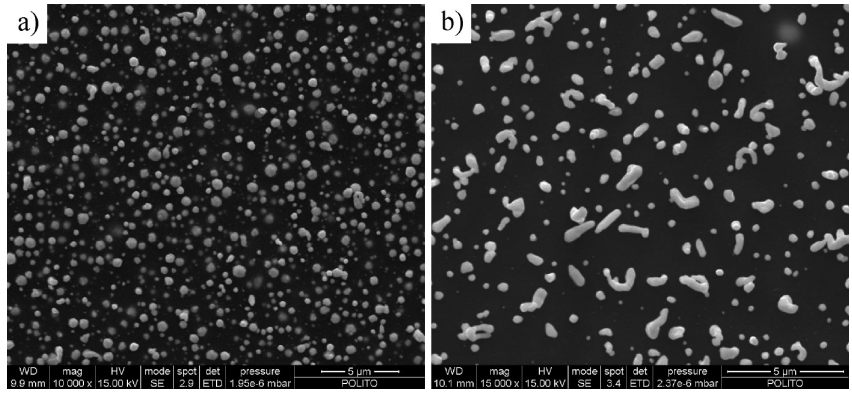

FIGURE 4. Comparison between the SEM micrographs of the bottom surfaces of (a) sample 1 and (b) sample 6.

Table 3. Summary of Bottom Surface SEM-EDX Analysis[a]

sample	remarks[b]	C:Ag (wt % ratio)	C:Ag (at % ratio)
1	nanoparticles of different sizes nearly equally distributed	50.93:49.07	90.31:09.69
2	same as above	48.37:51.63	89.38:10.62
3	same as above	51.52:48.48	90.52:09.48
4	same as above (more dense)	45.10:54.90	88.06:11.94
5	same as in 4	49.54:50.46	89.81:10.19
6	Ag particles have different shape and widely spaced	72.24:27.76	95.90:04.10
7	same as in 4	37.85:62.15	84.55:15.45

[a] An area of 5 μm × 5 μm was used for EDX analysis. [b] Readers may refer to Figure 4 for the corresponding SEM images.

A closer look reveals that for the first three samples, a mixture of silver nanocubes and agglomerates are formed on the top surfaces, whereas the other samples have more or less spherical nanoparticles and agglomerates (see Figure 2). This means that the formation of nanocubes occur at higher concentrations of pyrrole and silver nitrate. The nanocubes, nanoparticles and the agglomerates are of the order 100, 200 and 700 nm, respectively. Sample 6, which was prepared with NMP, instead of water + methanol mixture showed a very different topography, as depicted in Figure 3. The Ag particles were larger and were spaced widely apart compared to the other samples. Therefore, the solvent also plays a role in determining the structure and distribution of Ag particles. It should be noted that water and methanol are removed easily during the process of UV-curing, whereas NMP, which is a high boiling solvent, evaporates at a slower rate.

EDX analyses were also performed on these surfaces and the results are tabulated in Table 2.

The bottom surfaces (that were exposed to UV after the exposure of top surface) were more or less similar except, of course, sample 6. This is clearly evident from Figure 4, which shows the bottom surface of sample 1 (Figure 4a, representative for all the samples prepared in water + ethanol) and the bottom surface of sample 6 (Figure 4b, prepared in NMP).

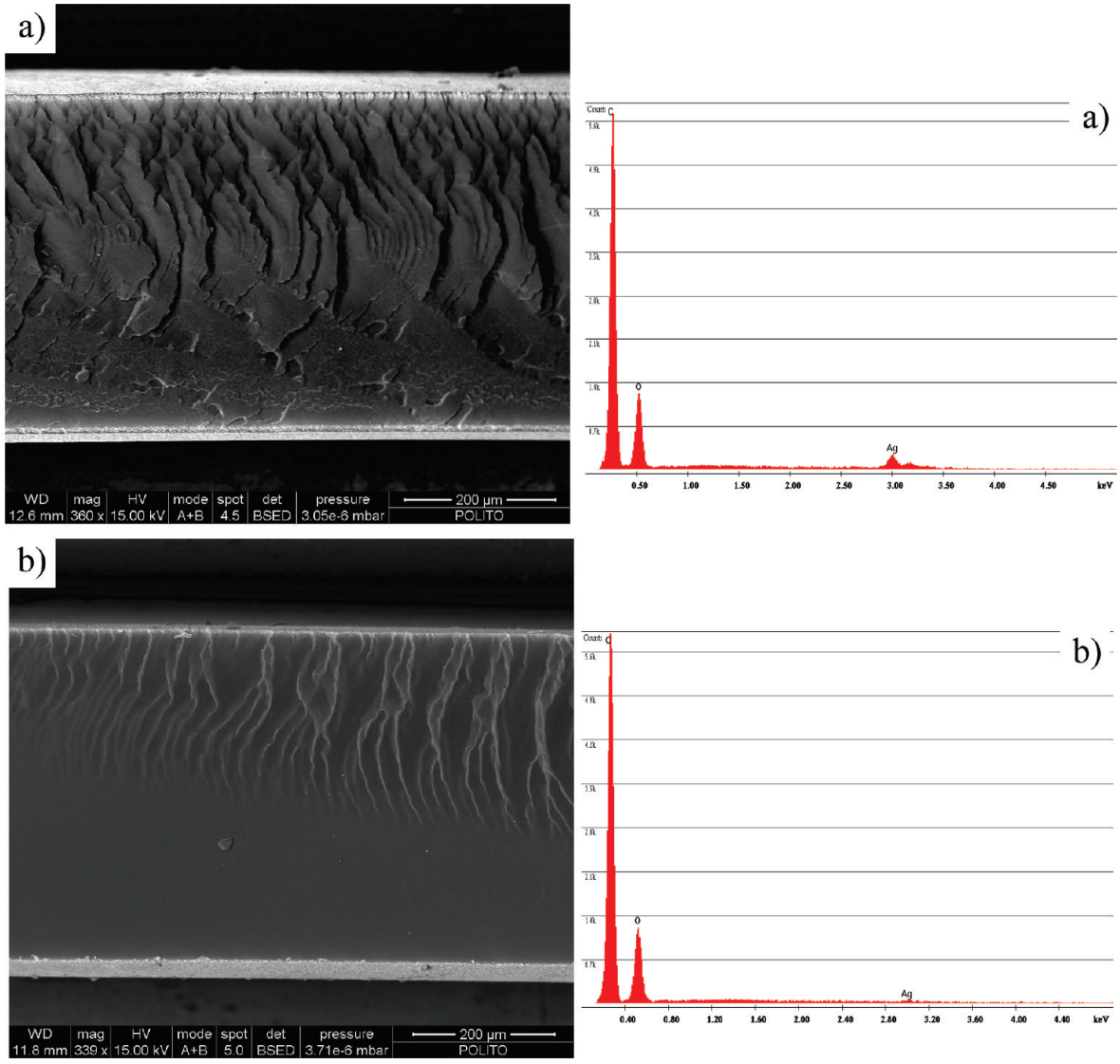

FIGURE 5. Cross-sectional SEM micrographs of (a) sample 2 and (b) sample 4. On the right is the corresponding EDX spectrum at center of the cross-section.

Table 4. Summary of Cross-Sectional SEM-EDX Analysis[a]

sample	remarks[b]	C:Ag (wt % ratio)	C:Ag (at % ratio)
1	silvered layer (~8 μm); Ag nanoparticles seen in center	85.88:14.12 [C] 60.11:39.89 [E]	98.20:01.80 [C] 92.84:06.88 [E]
2	silvered layer (~9 μm); Ag nanoparticles seen in center	90.62:09.38 [C] 59.08:40.92 [E]	98.86:01.14 [C] 92.84:07.16 [E]
3	silvered layer (~6.5 μm); some Ag nanoparticles seen in center	96.18:03.82 [C] 57.94:42.06 [E]	99.56:00.44 [C] 92.52:07.48 [E]
4	silvered layer (~4.5 μm); hardly any Ag nanoparticles seen in center	98.58:01.42 [C] 76.64:23.36 [E]	99.84:00.16 [C] 96.72:03.28 [E]
5	silvered layer (~4 μm); some Ag nanoparticles seen in center	97.35:02.65 [C] 76.91:23.09 [E]	99.65:00.35 [C] 96.77:03.23 [E]
6	silvered layer (~4.5 μm); some Ag nanoparticles seen in center	92.19:07.81 [C] 62.13:37.87 [E]	99.07:00.93 [C] 93.65:06.35 [E]
7	silvered layer (~3.5 μm); more Ag nanoparticles seen in center	84.24:15.76 [C] 71.59:28.41 [E]	97.96:02.04 [C] 95.77:04.23 [E]

[a] An area of 20 μm × 20 μm was used for EDX analysis. [b] Readers may refer to Figures 5 and 7 for the corresponding SEM images. [C] = center, [E] = edge.

The results of EDX analyses on the bottom surfaces are tabulated in Table 3. It is rather strange to note that the samples 4, 5, and 7 show higher density of Ag nanoparticles on both the surfaces though their formulations contained lesser amounts of $AgNO_3$ than for samples 1, 2, and 3. So, a cross-sectional analysis was necessary.

Figure 5 shows the cross-sections of samples 2 and 4. We clearly see the silvered layers on both sides with the polymer in between. SEM-EDX analysis was performed over an area of 20 μm × 20 μm at the center of the cross-section. EDX indicates a small amount of silver (see Figure 5a) in the center of sample 2 but practically nil at the center of sample 4 (Figure 5b). This represents a classical capacitor! Thus, formulation 4 provides an optimum mixture of reactants that allows for a clean separation of silver and pyrrole toward the surfaces.

Except for the anomalous behavior of sample 7, a comparison of the carbon to silver atomic ratios in both Table 2 and Table 3 demonstrates that sample 4 has more silver accumulated at both the surfaces, which indirectly suggests a much lower silver content in the center. This is also evident from Figure 5 and Table 4. In particular, Table 4 shows the carbon:silver ratios at the edges and at the center of the cross-sections of the samples.

A gradual decrease in the thickness of the silvered layers is seen from sample 1 to 7, which have decreasing amounts of pyrrole and $AgNO_3$. The separation of the silvered layer is not very clear in sample 6, made with NMP, and a number of Ag nanoparticles are seen throughout the cross-section (see Figure 6).

Sample 7 is prepared from very small amounts of pyrrole and $AgNO_3$; much of the silver particles are accumulated within a layer of about 3.5 μm, which explains the high ratio of Ag nanoparticles on its surface, as shown in Tables 2 and 3. For all the samples, the thicknesses of the silvered layers on both sides are almost same, and one such example is shown in Figure 7.

Though SEM-EDX analysis is not a rigorous quantitative technique, it does allow us to get a fair idea about the distribution of the particles and its associated properties.

Electrical Characterization and Capacitive Behavior. Current−voltage ($I-V$) curves were recorded for the surfaces of the samples to know how conductive they are. Figure 8 shows the I−V curves for the top surface of sample 2, which are perfectly linear, suggesting an ohmic behavior. Moreover, the overlapping of the five curves recorded over five different points on the surface indicates a highly homogeneous distribution of Ag nanoparticles and polypyrrole on the surface. Figure 9 is a graphical representation of the measured resistances of all samples, and it is seen that the surface resistance increases with a decrease in pyrrole and $AgNO_3$ contents, with the exception of sample 6 that showed a very high resistance (>100 KΩ).

Even though samples 5 and 6 contained the same amounts of pyrrole and $AgNO_3$, sample 6 was made with NMP instead of methanol + water mixture and hence has a different kind of distribution of Ag and polypyrrole causing a very high resistance. This asserts the importance of the medium of the reactive formulation. It is rather strange that though sample 7 showed a high density of Ag nanoparticles on its surface (vide supra), it also shows higher surface resistance compared to others. The reason could be that it has a much lower amount of polypyrrole, which forms conducting pathways all over the surface. A control sample with no pyrrole but 4 times the amount of $AgNO_3$ in sample 7 was prepared, and its resistance was found to be greater

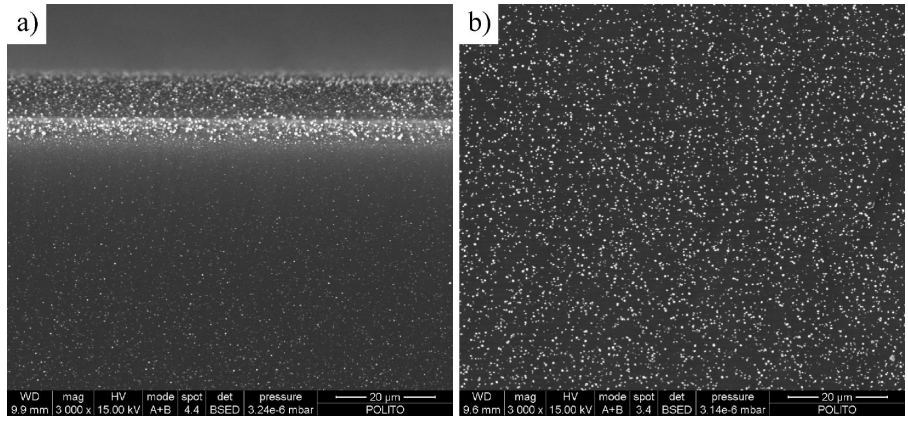

FIGURE 6. SEM micrographs of sample 6: (a) top edge and (b) central portion of the cross-section.

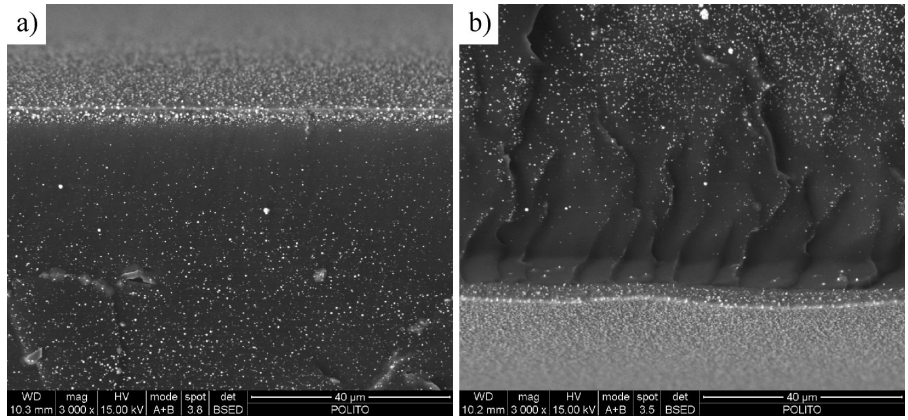

FIGURE 7. SEM micrographs of sample 7: (a) top edge and (b) bottom edge.

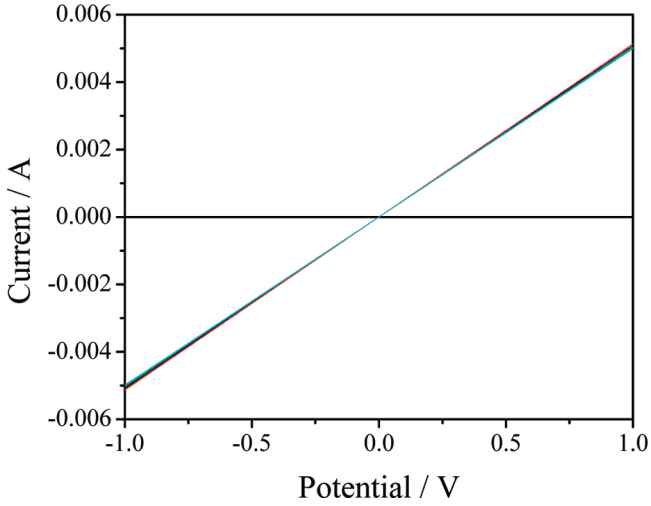

FIGURE 8. Current−voltage ($I-V$) plots recorded at five different locations on the top surface (exposed first) of sample 2 (average calculated resistance = 196 Ω).

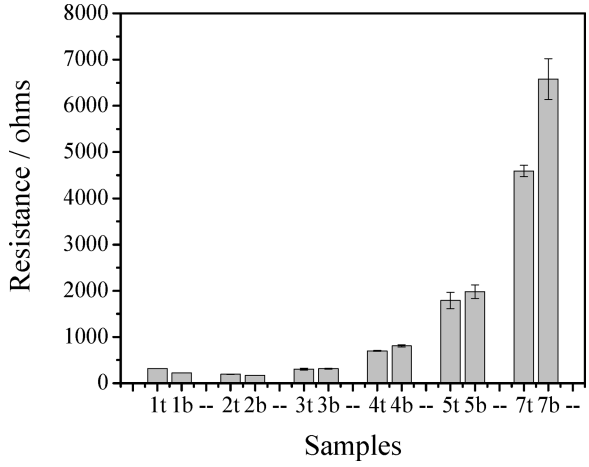

FIGURE 9. Comparison of the surface resistance values for the different samples prepared, measured with pin probes 1 cm apart. Sample 6 gave a very high value (>100 KΩ, not shown above). In the figure, "1t" means top surface of sample 1, "1b" means bottom surface of sample 1, and so on.

than 3 MΩ: this implies that both polypyrrole and Ag nanoparticles are essential for lowered resistances.

Further, electrical characterization involved AC Impedance Spectroscopy by varying the frequency from 100 kHz to 1 Hz. As an example, the complex plane plot for sample 2 shows the data points centered at 201 Ω along the real axis (Z'), and the Bode plot shows that there is no variation of resistance with change in frequency (see Figures S1 and S2 in the Supporting Information). This is clearly further evidence of ohmic behavior, which is in agreement with the results obtained from $I-V$ curves. Also, on switching the potentials, the current is instantly changed to a new value as determined by Ohm's law (see Figure S3 in the Supporting Information). The same is observed for all surfaces except for sample 6 (see Figure S4 in the Supporting Information). There is a considerable time delay in attaining a steady current value after the switch in potentials.

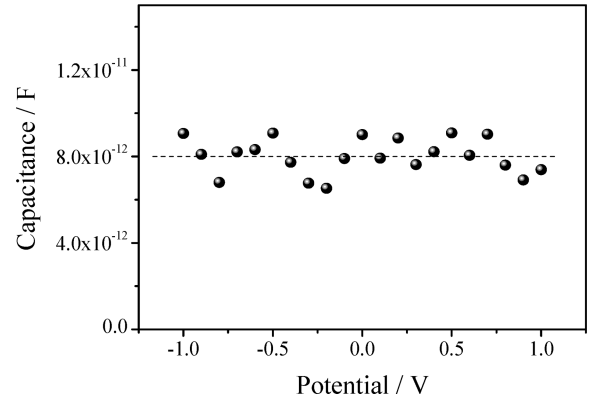

FIGURE 10. Capacitance vs voltage plot of sample 4 at frequency of 100 Hz (average value = 8 pF).

Circular discs of 1.0 cm in diameter were cut out from the master film and tested for capacitive properties. Figure 10 shows the capacitance vs potential curve for sample 4 at a frequency of 100 Hz. It is similar to the curve obtained by Liu et al. (21) for a polymeric capacitor prepared by inkjet printing with polyimide in the center and poly(3,4-ethylenedioxythiophene) on the surfaces, and the capacitance value is also similar, i.e., in the picofarad range.

Figure 11 shows the comparison of capacitance values of different samples, which shows large variations for different compositions. The higher values of capacitance obtained for the other samples, as compared to sample 4, are due to the Ag nanoparticles dispersed in the methacrylate polymeric matrix in the center. The polymeric coating on the Ag nanoparticles/agglomerates is the cause of such interesting phenomenon which is absent in classical bulk

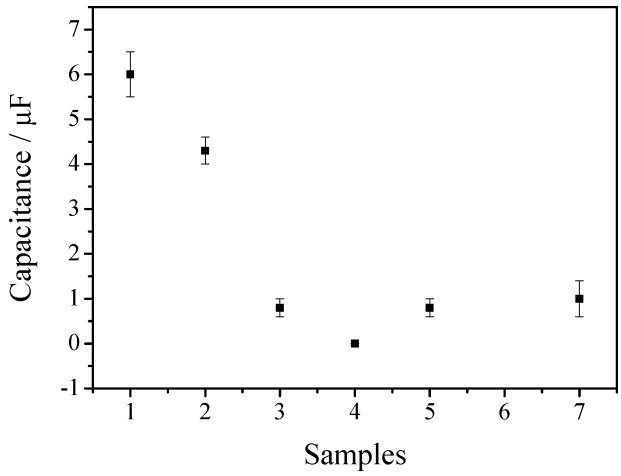

FIGURE 11. Comparison between the capacitance values of the different samples at frequency of 100 Hz; sample 6 gave a very high value of about 63 μF (not shown above).

metal−insulator capacitors. These nanoparticles, surrounded by polymeric material, form numerous nanocapacitors in the matrix causing higher capacitance (11, 12). The variance in capacitance values is quite large, and this is due to the different amounts of Ag being dispersed within the polymeric matrix.

Referring to Table 3, as obtained by SEM-EDX analysis, sample 1 shows the highest amount of silver in its formulation and a high Ag:C ratio in the center; correspondingly, it shows higher capacitance. Sample 2 has the same amounts of silver and pyrrole in its formulation but less solvent mixture, and hence the distribution of Ag particles is expected to be slightly different from sample 1. This is reflected in the lower Ag:C ratio in the center and little lower capacitance, as shown in Figure 8b. Samples 3 and 5 have even lower Ag:C ratio, and their capacitances are correspondingly lower. Sample 4 has almost no silver in the center and behaves like a classical capacitor with conducting-insulating interfaces. On the other hand, sample 6 shows a drastically large capacitance (about 10 times more than sample 1). It is not surprising, considering the fact that it was made from a different solvent (i.e., NMP instead of methanol + water mixture). Moreover, we also see (SEM images discussed above) a different kind of particle distribution and morphology for sample 6.

Proposed Mechanism. The formation of metallopolymer capacitors described above is due to the surface migration of silver during polymerization under UV exposure. The formation of silvered layers on both surfaces indicates that there is migration of silver ions and pyrrole toward both surfaces under UV irradiation. From complexation studies and the "hard and soft acid-base" (HSAB) concept (22, 23), it is known that transition metal ions (e.g., silver) being a soft acid would form stronger complex with nitrogen-containing pyrrole than the polyether oxygen of BEMA, and hence both silver and pyrrole migrate together to the surfaces. The causes for such migration are not fully clear yet. We hypothesize that since the photoinitiated reaction of BEMA (17) is much faster than the redox reactions of pyrrole and Ag^+, the formation of cross-linked BEMA polymer pushes out the Ag^+ and pyrrole contained in aqueous domains. As the silver ions and pyrrole are converted at the surface, the concentration gradient also might drive them toward the surface. Further evidence is gained by the observation of films after about one hour of photopolymerization (see Figure S5a,b in the Supporting Information). The films with formulations 1 to 3 turned black within about 6 to 10 min of initial exposure to UV; but samples 5−7 remained orange/brown for some hours, getting darker with passage of time. As seen from the same Figure S5b, the methacrylate film is already formed within 6 min of UV exposure, but the redox reactions between Ag^+ and pyrrole continue to go on slowly after the initial exposure. These samples had lesser amounts of $AgNO_3$ and pyrrole and hence the redox reactions were slower. The slowest was in case of sample 7, which had the smallest amounts of $AgNO_3$ and pyrrole. Even though the sample looked black after about 8 h, its surface resistance decreased over a period of week (the value reported in Figure 7b is the stabilized value after 7 days).

As another control experiment, a film with formulation of sample 2 was prepared by exposing only one side. Several Ag nanoparticles were seen only on the exposed side by SEM (as seen for samples 2 to 5) and very few on the unexposed side. Concurrently, the unexposed side also exhibited a very high resistance. The second side was exposed to UV after 2 days and observed under SEM. There was no change in the morphology or in the resistance. This implies that the migration of silver occurs during polymerization and it is important to expose both sides within a suitable short time gap so that migration occurs on both the sides. The same reasoning can be extended to sample 6 made with NMP. In this case there is less migration because the silver ions can be associated with nitrogen of NMP as well as pyrrole. So, even though the samples 5 and 6 were made from same amounts of silver and pyrrole, sample 5 has less silver in the center compared to sample 6 (see Table 3) and more on the surfaces (see Tables 1 and 2). Consequently, sample 6 has a very high surface resistance, but more Ag−polymer nanocomposites in the bulk, leading to a very high capacitance.

Southward and Stoakley reported the observation of such migration of silver in thermally cured polyimides, and it seemed there was still no explanation as to why and how it happens (2). However, in their papers on Pd metalized polymer surfaces, they argue that the development of a metalized film surface from atom/cluster migration to the surface within an organic macromolecular matrix is unexpected because metal atoms and nanoclusters produced in the thermal cycle must remain within the bulk of the polymer (24, 25). That is, the high surface free energy of metal particles relative to organic materials (about 10:1) thermodynamically precludes a metal surface developing via atom/cluster migration from the bulk to the surface of the polymer film. They suggest an alternative mechanism based on aggregation due to sintering and ripening during thermal curing cycles. They state that a conducting metalized film is formed only after being held at 300 °C for 1 h, during which

at least 17% of polyimide is lost and the metal content increases proportionately. Indeed, no metallization was observed for their films held at 275 °C even for 5 h, and no metallization was observed on the air-protected glass side of the film. Thus, they concluded that the emergence of a Pd surface proceeds with (and is dependent on) concomitant oxidative degradation of polyimide to all or mostly volatile products, that are temperature and atmosphere (oxygen) dependent. Our conditions are quite different, i.e., the temperature of the mixtures was always found to be below 40 °C because of the flow of nitrogen above the samples during UV curing. This temperature is way below the thermal decomposition of BEMA, which occurs at approximately 300 °C (17). Hence, it is the solvent, reactants, and time factors as explained above that are fundamental in our method of preparing surface metalized films by UV curing.

CONCLUSIONS

In summary, we have successfully introduced a novel, simple but efficient method that allows excellent dual surface metallization of a methacrylic-based polymer network, in a single step. The formation of two conducting layers on either sides of an insulating polymer in a single step opens up possibilities of rapid production of highly flexible polymeric capacitors, which until now are made by time-consuming multiple steps procedures. The whole process is remarkably convenient, with short reaction time, "environmentally friendly", and no need for any complex equipment or manipulation. It would be of further interest to fine-tune the formulations and experimental conditions to get films with predetermined capacitances. Further work is in progress to have a deeper understanding of the mechanism of migration of Ag^+, and to extend the technique to other metals and polymer matrices.

Acknowledgment. V.S.I. thanks Italian Regione Piemonte Council for the research grant. The authors would like to thank Mr. Mauro Raimondo for the SEM-EDX analysis of the samples.

Supporting Information Available: Electrical characterization by means of AC Impedance Spectroscopy (Nyquist & Bode plots); effect of switching potentials on current; photographs of the films after UV exposure (PDF). This material is available free of charge via the Internet at http://pubs.acs.org.

REFERENCES AND NOTES

(1) Southward, R. E.; Thompson, D. W. *Adv. Mater.* **1999**, *11*, 1043–1047.
(2) Southward, R. E.; Stoakley, D. M. *Prog. Org. Coat.* **2001**, *41*, 99–119.
(3) Warner, J. D.; Pevzner, M.; Dean, C. J.; Kranbuehl, D. E.; Scott, J. L.; Broadwater, S. T.; Thompson, D. W.; Southward, R. E. *J. Mater. Chem.* **2003**, *13*, 1847–1852.
(4) Tee, D. I.; Mariatti, M.; Azizan, A.; See, C. H.; Chong, K. F. *Compos. Sci. Technol.* **2007**, *67*, 2584–2591.
(5) Davis, L. M.; Thompson, D. S.; Dean, C. J.; Pevzner, M.; Scott, J. L.; Broadwater, S. T.; Thompson, D. W.; Southward, R. E. *J. Appl. Polym. Sci.* **2007**, *103*, 2409–2418.
(6) Li, Y.; Lu, Q.; Qian, X.; Zhu, Z.; Yin, J. *Appl. Surf. Sci.* **2004**, *233*, 299–306.
(7) Andreescu, D.; Wanekaya, A. K.; Sadik, O. A.; Wang, J. *Langmuir* **2005**, *21*, 6891–6899.
(8) Li, S.; Gong, S. *Adv. Funct. Mater.* **2009**, *19*, 2601–2606.
(9) Southward, R. E.; Thompson, D. W. *Materials and Design* **2001**, *22*, 565–576.
(10) Pothukuchi, S.; Li, Y.; Wong, C. P. *J. Appl. Polym. Sci.* **2004**, *93*, 1531–1538.
(11) Shen, Y.; Lin, Y.; Nan, C.-W. *Adv. Funct. Mater.* **2007**, *17*, 2405–2410.
(12) Qi, L.; Lee, B. I.; Chen, S.; Samuels, W. D.; Exarhos, G. J. *Adv. Mater.* **2005**, *17*, 1777–1781.
(13) Qi, S.; Wu, Z.; Wu, D.; Wang, W.; Jin, R. *Chem. Mater.* **2007**, *19*, 393–401.
(14) Rubira, A. F.; Rancourt, J. D.; Taylor, L. T.; Stoakley, D. M.; Clair, A. K. S. *J. Macromol. Sci., Pure Appl. Chem.* **1998**, *35*, 621–636.
(15) Qi, S.-L.; Wang, W.-C.; Wu, D.-Z.; Wu, Z.-P.; Jin, R.-G. *Eur. Polym. J.* **2006**, *42*, 2023–2030.
(16) Southward, R. E.; Thompson, D. W. *Chem. Mater.* **2004**, *16*, 1277–1284.
(17) Nair, J. R.; Gerbaldi, C.; Meligrana, G.; Bongiovanni, R.; Bodoardo, S.; Penazzi, N.; Reale, P.; Gentili, V. *J. Power Sources* **2008**, *178*, 751–757.
(18) Nair, J. R.; Gerbaldi, C.; Chiappone, A.; Zeno, E.; Bongiovanni, R.; Bodoardo, S.; Penazzi, N. *Electrochem. Commun.* **2009**, *11*, 1796–1798.
(19) Gerbaldi, C.; Nair, J. R.; Ahmad, S.; Meligrana, G.; Bongiovanni, R.; Bodoardo, S.; Penazzi, N. *J. Power Sources* **2010**, *195*, 1706–1713.
(20) Ijeri, V. S.; Nair, J. R.; Gerbaldi, C.; Gonnelli, R. S.; Bodoardo, S.; Bongiovanni, R. M. *Soft Matter* **2010**, *6*, 4666–4668.
(21) Liu, Y.; Cui, T.; Varahramyan, K. *Solid-State Electron.* **2003**, *47*, 1543–1548.
(22) Ijeri, V. S.; Srivastava, A. K. *J. Chem. Eng. Data* **2002**, *47*, 346–350.
(23) Ijeri, V. S.; Srivastava, A. K. *Eur. J. Inorg. Chem.* **2001**, 943–947.
(24) French, B. L.; Davis, L. M.; Munzinger, E. S.; Slavin, J. W. J.; Christy, P. C.; Thompson, D. W.; Southward, R. E. *Chem. Mater.* **2005**, *17*, 2091–2100.
(25) Davis, L. M.; Compton, J. M.; Kranbuehl, D. E.; Thompson, D. W.; Southward, R. E. *J. Appl. Polym. Sci.* **2006**, *102*, 2708–2716.

AM1006639